A study on the corrosion fatigue behaviour of laser-welded shape memory NiTi wires in a simulated body fluid

Chan, C-W. (2017). A study on the corrosion fatigue behaviour of laser-welded shape memory NiTi wires in a simulated body fluid. *Surface and Coatings Technology*, *320*, 574-578.
https://doi.org/10.1016/j.surfcoat.2016.10.094

Published in:
Surface and Coatings Technology

Document Version:
Peer reviewed version

Queen's University Belfast - Research Portal:
Link to publication record in Queen's University Belfast Research Portal

A study on the corrosion fatigue behaviour of laser-welded shape memory NiTi wires in a simulated body fluid

Chi-Wai Chan

PII: S0257-8972(16)31091-X
DOI: doi: 10.1016/j.surfcoat.2016.10.094
Reference: SCT 21739

To appear in: *Surface & Coatings Technology*

Received date: 16 August 2016
Revised date: 30 October 2016
Accepted date: 31 October 2016

Please cite this article as: Chi-Wai Chan, A study on the corrosion fatigue behaviour of laser-welded shape memory NiTi wires in a simulated body fluid, *Surface & Coatings Technology* (2016), doi: 10.1016/j.surfcoat.2016.10.094

A Study on the Corrosion Fatigue Behaviour of Laser-welded Shape Memory NiTi Wires in a Simulated Body Fluid

Chi-Wai CHAN

Bioengineering Research Group, School of Mechanical and Aerospace Engineering, Queen′s University Belfast, BT9 5AH, UK

Corresponding Author: c.w.chan@qub.ac.uk

Keywords: Laser welding, shape memory alloys, NiTi, corrosion fatigue, Hanks' solution

Abstract

Corrosion fatigue is a fracture process as a consequence of synergistic interactions between the material microstructure, corrosive environment and cyclic loads/strains. It can cause unexpected failure of medical and dental implants in the human body. This study reveals a comparison of corrosion fatigue behaviour between shape memory NiTi wire and its laser weldment using bending rotation fatigue (BRF) test integrated with a specifically-designed corrosion cell. The testing medium was Hanks' salt solution kept at 37.5 ^{o}C. Electrochemical impedance spectroscopic (EIS) measurement was carried out to monitor the change of corrosion resistance of the samples during the BRF tests at different periods of immersion time in Hanks' solution. Scanning electron microscopy (SEM) was used to analyse the fracture surfaces. This study provides important information on the susceptibility of NiTi alloy and its weldment to corrosion fatigue in Hanks' solution.

1. Introduction

The unique shape memory effect (SME) and superelasticity (SE) coupled with excellent corrosion resistance and biocompatibility make the equiatomic NiTi alloy desirable for biomedical applications. The SME, which is a thermally-induced effect, refers to the ability of a deformed NiTi to return to its pre-deformed shape upon heating. This characteristic is desirable for making bone staples to fasten fractured bones [1]. The SE, which is a stress-induced effect, refers to the ability to recover a large amount of strain (up to 8%) in an elastic manner when stress is released. This characteristic is highly desirable for making cardiovascular stents and dental arch wires [1]. Both the SME and SE are the consequences of diffusionless phase transformation between the austenite and martensite phases.

Fatigue fracture is one of the major concerns for the NiTi medical and dental implants. Fatigue-related mechanisms have been reported to be responsible for majority of mechanical failures of implantable medical metallic components [2]. Fatigue fracture can also be assisted by different types of corrosion, such as anodic dissolution or hydrogen embrittlement. The cracking of materials under the synergistic effects of cyclic loadings and corrosion is called corrosion fatigue. Corrosion fatigue can cause the medical and dental implants to fail prematurely. Considering a NiTi stent as an example, it is inevitably exposed to cyclic stresses/strains and may suffer from fatigue in the *in vivo* physiological environment. Premature fracture of the NiTi stent due to corrosive fatigue is highly dangerous, in addition to releasing toxic Ni ions into the surrounding tissue. It is reported that 4.5-8 % of the general population is hypersensitive to Ni [3, 4]. Release of the Ni ions can lead to up-regulation of inflammatory mediators and promote in-stent restenosis [5].

The protection of NiTi surface against anodic corrosion or hydrogen embrittlement relies heavily on the surface oxide film which is principally amorphous TiO_2 with small amounts of Ti sub-oxides (TiO and Ti_2O_3) and Ni oxidized species [6]. It acts as a strong barrier to protect the NiTi surface from the corrosive species (e.g. Cl^-) or hydrogen ingress in Hanks' solution. Furthermore, it is known that the characteristics of the oxide film on NiTi can be significantly altered by fabrication

process [7]. Such changes can be either beneficial or harmful to NiTi depending on the type of process and processing conditions.

A commercial method to fabricate the NiTi stent is by laser cutting a pattern from a NiTi sheet, rolling it up and welding at specific strut locations [8]. The welded structure of the strut is liable to the corrosion fatigue because of the following: (i) changes of surface oxide film characteristics, (ii) presence of surface irregularities and welding defects (i.e. acting as crack initiation sites of fatigue) and (iii) susceptibility to galvanic corrosion due to the microstructural and composition differences or inhomogeneity in the weld zone (WZ), heat-affected zone (HAZ) and base metal (BM). However, existing studies in literature focus mainly on either corrosion or fatigue of the NiTi alloy. The first representative study on the mechanical fatigue properties of laser-welded NiT wires was done by Yan *et al.* [9]. They studied the mechanical fatigue using bending rotation fatigue (BRF) method. They also investigated the effect of post-weld heat-treatment on the mechanical fatigue in their subsequent study [10]. Chan *et al.* [11] reported the fatigue fracture mechanisms of NiTi laser joints when subject to small strain in BRF. Panton *et al.* [12, 13] investigated the thermomechanical fatigue properties of laser-welded and post-weld heat-treated NiTi wires using a custom design setup. On the other hand, Yan *et al.* [14, 15] studied the corrosion properties of laser-welded NiTi wires in 0.9 % NaCl solution and Hanks' solution at different pH values, in addition to their work on mechanical fatigue. Chan *et al.* [6] investigated the corrosion properties of post-weld heat-treated NiTi laser joints in Hanks' solution. Mirshekari *et al.* [16] studied the effect of laser welding on the microstructure and corrosion resistance of NiTi wires in Ringer's solution. Pequegnat *et al.* [17] characterised the surfaces of laser processed NiTi alloys and reported their corrosion and Ni ion release performance in phosphate buffered saline (PBS) solution.

It is the first time to report on the corrosion fatigue behaviour of NiTi alloy and its weldment in Hanks' solution. Particular focus is devoted to elucidate the role of surface oxide films on NiTi in the corrosion fatigue process in Hanks' solution.

2. Experimental Details

2.1. Laser Welding Experiment

The materials used were commercial Ti-55.91 wt % NiTi wires with diameter of 0.5 mm (procured from Johnson Matthey Noble Metals). The laser-welded sample was prepared by laser welding two NiTi wires using a SPI continuous wave (CW) fiber laser (SPI Lasers UK Ltd, UK). The wavelength of laser is 1091 nm. The wire surface was ground by a series of sandpapers up to 600 grit before laser welding. The laser processing parameters were determined from a previous optimization study [18]. The laser power was 72 W, welding time was 115 ms, and focus position was at the surface (+ 0 mm defocusing). The laser welding experiments were conducted in Ar shielding environment with the flow rate of 25 L/min. The characteristics for BM and WZ in the NiTi laser joints obtained in previous studies [6, 11, 18] are summarised in Table 1.

2.2. Setup of Corrosion Fatigue Test in Hanks' Solution

The fatigue life of the as-received and laser-welded wire samples was measured using a specifically-designed test rig based on the concept of bending rotation fatigue (BRF) test. Interested readers are referred to [11] for design of the test rig and details of the BRF test. The key parameters of the BRF test, such as rotational speed and surface strain were controlled at 100 rpm (or 1.67 Hz) and 0.42 % respectively. To mimic the human body conditions, a fixed portion of the bended wire sample was immersed in a corrosion cell filled with 250 mL of Hanks' solution during the BRF test. The Hanks' solution was continuously pumped from a container immersed in a temperature-controlled water bath kept at 37.5 ^{o}C. The composition of Hanks' solution is: NaCl 8 g/L, Na_2HPO_4 0.0475 g/L, $NaHCO_3$ 0.35 g/L, KCl 0.4 g/L, KH_2PO_4 0.06 g/L, $MgCl_2$-$6H_2O$ 0.10 g/L, $MgSO_4$-$7H_2O$ 0.10 g/L, $CaCl_2$ 0.18 g/L, glucose 1 g/L, pH 7.4. The samples used in the corrosion fatigue test were

mechanically ground using sandpapers up to 2400 grit, and then ultrasonically degreased and cleaned by acetone and distilled water for 10 min respectively. The surface area of the wire sample exposed to Hanks' solution was controlled at 0.5 cm^2. The samples tested in air were used as control for comparison. The fracture surfaces after the corrosion fatigue test were captured using scanning electron microscope (SEM, Model JSM-6490, JEOL).

2.3. Monitoring of Corrosion Resistance during Corrosion Fatigue Test

The corrosion resistance of the as-received and laser-welded samples during the corrosion fatigue test was monitored by electrochemical impedance spectroscopy (EIS). The EIS measurements were carried out by means of a frequency response detector coupled to the PAR 273A potentiostat. A standard calomel electrode (SCE) was used as the reference electrode and a platinum wire gauze was used as the counter electrode. The EIS data were collected at different measurement time points, namely 1h, 8h, 24h, 48h, 72h, 96h and 120h. During each measurement, a sine wave of 10 mV in amplitude was applied to the wire sample at open-circuit potential (OCP). The impedance spectra were acquired in the frequency range from 100 kHz to 1 mHz. The EIS data were fitted to an equivalent circuit using the software ZSimpWin.

3. Results and Discussion

3.1. Fatigue Life Measurement in Air and Hanks' Solution

The fatigue life of the as-received and laser-welded samples tested by BRF in air and Hanks' solution are presented in Fig. 1. The error bars indicate the standard deviation of the mean (number of samples = 5). As observed in Fig. 1, the fatigue life of the as-received sample tested in air is longer than that tested in Hanks' solution. However, the difference is not significant given that error bars overlap with each other. In contrast, the laser-welded sample tested in Hanks' solution shows a notable

reduction in fatigue life when compared with that tested in air. This indicates that NiTi wire is highly susceptible to corrosion fatigue in Hanks' solution after laser welding. It is important to note that the fatigue fracture mechanisms of the as-received and laser-welded samples tested in air, including the effects of welding defects on cracking mechanisms, have been reported in detail in a previous publication [11].

3.2. Fracture Surface Analysis by SEM

Fig. 2 (a-d) shows the fracture surfaces of the as-received and laser-welded samples after tested by BRF in Hanks' solution. As observed in the figures, numerous micro-cracks appeared in the fracture surfaces of the as-received (Fig. 2 (a-b)) and laser-welded samples (Fig. 2 (c-d)). Such micro-cracks are absent from the samples (both as-received and laser-welded) tested in air (refers to [11]). In addition, striations (i.e. standard signs of fatigue fracture) can be observed from the laser-welded sample tested in Hanks' solution (Fig. 2d). SEM fractography analysis indicates that the fracture surfaces of the as-received and laser-welded samples are free from corrosion pits (i.e. signs of anodic corrosion), but with the presence of micro-cracks (i.e. signs of environmental attack by hydrogen). This points to the fact the reduction of fatigue life is attributable to the damage associated with hydrogen embrittlement rather than anodic dissolution. Taking the results of the fatigue life measurements into consideration, NiTi wire is also affected by hydrogen embrittlement in Hanks' solution when subjected to fatigue loads/strains, but the effect is not as significant as that after laser welding.

3.3. Oxide Film Monitoring in Hanks' Solution by EIS

Fig. 3 shows the Nyquist plots of impedance spectra for the as-received and laser-welded samples tested by BRF in Hanks' solution with different immersion periods. The Nyquist plots are used to monitor the change of polarization resistance of oxide films with increasing immersion time (i.e.

before fatigue fracture of the samples). The diameter of the Nyquist semicircle reveals the polarization resistance (R_p). In the present study, the R_p value is estimated by fitting the EIS data to an equivalent electrical circuit model, namely Randles circuit. The Randles circuit includes a solution resistance (R_s) in series with a parallel combination of polarization resistance (R_p) and capacitance of the oxide film. It should be noted that the capacitor is not ideal and behaves like a constant phase elements (CPE). The reciprocal capacitance of the oxide film is proportional to the film thickness [19]. The Randles circuit is shown in the inset of Fig. 3. Table 2 shows the values of fitted parameters of the equivalent circuit for the as-received and laser-welded samples using ZSimpWin.

The EIS results indicate that the polarization resistance of oxide films for both samples increases between 1h and 24h of immersion in Hanks' solution, and subsequently declines between 24h and 120h (for the as-received sample) and between 24h and 72h (for the laser-welded sample). The laser-welded sample fractured before the measurement time point of 120h. The CPE of oxide film for the as-received sample falls within the range of 72.4 to 78.4 uF/cm^2 throughout the entire immersion periods (from 1h to 120h), while the CPE for the laser-welded sample decreases from 68.2 to 56.9 uF/cm^2 (from 1h to 72h). The value of *n*, varying from 0 to 1, is dependent on the surface roughness and integrity of oxide film for a corrosion system. For $n = 1$, the CPE represents a pure capacitor. The n values of the as-received and laser-welded samples lie between 0.90 and 0.93, indicating a near capacitive behaviour of the oxide films.

If no mechanical stress is applied, the equilibrium of the corrosion system depends on the exchange of ions at electrolyte/metal interface in two opposite processes, i.e. film dissolution and film thickening. When conducting the BRF tests in Hanks' solution, the case is much more complex in that the oxide film undergoes repetitive film rupture and repassivation processes. It is believed that the change of polarization resistance of oxide films during the corrosion fatigue tests is primarily attributable to the change of oxide composition as a consequence of film rupture and repassivation. Film thickening does not contribute much to the remarkable change in polarization resistance given that

the capacitance (indicating the film thickness) of the as-received sample only changes slightly over time.

3.4. Repassivation of Oxide Film and Hydrogen Ingress in Hanks' Solution

When NiTi reacts with aqueous solution at OCP, a nanometer thick oxide film which is principally amorphous TiO_2 immediately forms on the surface [6]. The cyclic tensile-compressive bending actions during the BRF tests cause repetitive rupture and repassivation of the oxide film. Rupture of the oxide film exposes the bare metal to the electrolyte, but shortly after this, repassivation takes place and repairs the ruptured film. The repassivation process involves generation of hydrogen ions. In the subsequent reduction, the hydrogen ions will transform into hydrogen atoms and molecules which are the main source to initiate the hydrogen embrittlement in metal. The mechanisms for the hydrogen embrittlement in NiTi are schematically explained in Fig. 4. It is important to note that the hydrogen barrier properties of the oxide depend on the oxide composition and integrity. The composition of oxide film of NiTi can be altered by Hanks' solution as explained below.

Firstly, the regenerated oxide film can react with hydrogen during repassivation. Hydrogen absorption in the oxide film can induce a change in the oxide composition (i.e. TiO_2 ➔ TiOOH). The redox transformations, namely Ti (IV) ➔ Ti (III), within the oxide film can lead to the increase in the film conductivity [20]. In addition, the presence of Ti(III) in the film in forms of either TiOOH or Ti_2O_3 suboxides makes the oxide film not as stable and protective as the Ti (IV), i.e. TiO_2. Ti (III) species are generally considered as defects in the passive film [21]. The hydrogen atoms can enter the metal through the conductive and defective pathways in the oxide. Secondly, the repassivation of Ti in Hanks' solution is reported to be more sluggish than that in saline [22], which in turn indicates that the oxide film has more time to react with hydrogen to form TiOOH during the film healing process, rendering the oxide film less resistant to hydrogen ingress. Finally, the regenerated oxide film can also

react with the Ca and P ions in Hanks' solution to form calcium phosphate or calcium titanium phosphate in the outermost layer [22]. It has been reported that such Ca or P containing layer is not an effective anticorrosion layer [23].

It is worthy to note that the fracture occurred in the WZ, not HAZ even though HAZ has larger grain size, i.e. smaller grain-boundary area due to larger grain size enhances the uptake of cathodic hydrogen atoms [24]. This can be attributed to the presence of welding defects in the WZ, such as porosities [11]. The cathodic atomic hydrogen can diffuse through the WZ surface and reach the porosities to form molecular hydrogen. High local pressure can be built up inside the pores and burst the pores to result in brittle fracture.

The differences in fatigue life of the samples tested in air and Hanks' solution can be explained by the proposed mechanism in Fig. 4 together with the following two chemical equations:

For Ti: $Ti + 2H_2O \rightarrow TiO_2 + 4H^+ + 4e^-$

For Ni: $Ni + H_2O \rightarrow NiO + 2H^+ + 2e^-$ or $Ni + 2H_2O \rightarrow Ni(OH) + 2H^+ + 2e^-$

When testing in air, the cracking mechanisms of the samples are purely mechanical, with the as-received sample being more fatigue-resistant than the laser-welded counterpart (refers to Fig. 1). When testing in Hanks' solution, the hydrogen ions generated from the chemical reactions between the metals (Ni and Ti) and H_2O deteriorate the passive film properties and the resulting H_2 molecules interfere with the microstructural and/or weld defects of the samples, rendering the cracking mechanisms from purely mechanical to a mixture of mechanical and microstructural, i.e. hydrogen embrittlement. The samples become less fatigue-resistant and more brittle when compared to those tested in air (refer to Fig. 1), with the laser-welded sample being more susceptible to hydrogen embrittlement than the as-received sample.

4. Conclusions:

In this study, the corrosion fatigue behaviour of NiTi wire and its weldment in Hanks' solution at 37.5 ^{o}C was carefully compared and analysed. The following conclusions were reached:

1. Laser-welded NiTi wire tested in Hanks' solution showed a notable reduction in fatigue life;
2. Reduction of fatigue life is attributed to the damage associated with hydrogen embrittlement;
3. Change of polarization resistance of oxide films during the corrosion fatigue tests is primarily attributed to the change of oxide composition as a consequence of film rupture and repassivation;
4. Fatigue fracture occurred in the weld zone (WZ) of the laser-welded NiTi.

Acknowledgement

The work described in this paper was supported by the Queen's University Belfast (Start-up Research Fund: D8201MAS), United Kingdom.

References:

[1] A. Kapanen, *et al.*, *Biomaterials*, 23 (2002) 645-650.

[2] R.T. Antunes and M. Oliveira, *Acta Biomaterialia*, 8(3) (2012) 937-962.

[3] L. Peltonen, Contact Dermatitis, 5 (1979) 27-32.

[4] H. Hildebrand, *et al.*, *Biomaterials*, 10 (1989) 545-548.

[5] D.O. Halwani, *et al.*, *Journal of Invasive Cardiology*, 22(11) (2010) 528-535.

[6] C.W. Chan, *et al.*, *Corrosion Science*, 56 (2012) 158-167.

[7] M.H. Wong, *et al.*, *Journal of Alloys and Compounds*, 466 (2008) L5–L10.

[8] D. Stoeckel, *et al.*, *European Radiology*, 14(2) (2004) 292-301.

[9] X.J. Yan, *et al.*, *Materials Characterization*, 57(1) (2006) 58-63.

[10] X.J. Yan, *et al.*, *Materials Characterization*, 58(3) (2007) 262-266.

[11] C.W. Chan, *et al.*, *Materials Science and Engineering A*, 559 (2013) 407-415.

[12] B. Panton, *et al.*, The effect of laser welds on the thermomechanical fatigue of NiTi shape memory alloys' ASME 2014 Conference on Smart Materials, Adaptive Structures and Intelligent Systems, Newport, Rhode Island, USA, *American Society of Mechanical Engineers*.

[13] B. Panton, *et al.*, *International Journal of Fatigue*, 92 (2016) 1-7.

[14] X.J. Yan and D.Z. Yang, *Journal of Biomedical Materials Research Part A*, 77(1) (2006) 97-102.

[15] X.J. Yan, *et al.*, Materials Characterization, 58(7) (2007) 623-628.

[16] G.R. Mirshekari, *et al.*, *Journal of Materials Engineering and Performance*, 24(9) (2015) 3356-3364.

[17] A. Pequegnat, *et al.*, *Materials Science and Engineering C*, 50 (2015) 367-378.

[18] C.W. Chan, *et al.*, *Lasers in Engineering*, 30(3-4) (2015) 247-265.

[19] I. Milosev, *et al.*, *Electrochimica Acta*, 53 (2008) 3547-3558.

[20] M. Vezvaie, *et al.*, *Journal of the Electrochemical Society*, 160(9) (2013) C414-C422.

[21] Z. Qin, *et al.*, *Applied Surface Science*, 303 (2014) 282-289.

[22] G. Manivasagam, *et al.*, *Recent Patents on Corrosion Science*, 2 (2010) 40-54.

[23] E.K. Cydzik, *Journal of Achievements in Materials and Manufacturing Engineering*, 43(1) (2010) 424-431.

[24] R.H. Jones, Stress Corrosion Cracking, ASM International, Materials Park, Ohio, 1992.

Tables and Figures

Table 1 – Summary of characteristics for base metal (BM) and weld zone (WZ) in the NiTi laser joints (refer the details in [6], [11] and [18])

Characteristics		Base metal (BM)	Weld zone (WZ)
Microstructure (at room temperature) [18]		B2 austenite with no precipitate	B2 austenite with no precipitate
Grain size [11, 18]		Equiaxed grains (in nanometer range)	Columnar dendrites (about 1-3 μm)
Transformation temperature [18]	Austenite start (A_s)	2.4 °C	-25.4 °C
	Austenite finish (A_f)	19.8 °C	-12.3 °C
	Martensite start (M_s)	13.8 °C	-43.2 °C
	Martensite finish (M_f)	-6.3 °C	-56.4 °C
Vickers micro-hardness [18]		339 HV	277 HV
Corrosion parameters (tested in Hanks' solution at 37.5 °C) [6]	Corrosion potential (E_{corr})	-312 mV_{SCE}	-335 mV_{SCE}
	Pitting potential (E_{pit})	317 mV_{SCE}	278 mV_{SCE}
	Corrosion current (I_{corr})	0.46 $\mu A/cm^2$	0.52 $\mu A/cm^2$

Table 2 – Values of fitted parameters of the equivalent circuit for the as-received and laser-welded samples after testing by BRF in Hanks' solution with different immersion times

Sample	Immersion Time	R_s (Ω cm^2)	CPE (μF/cm^2)	n	R_p (MΩ cm^2)
As-received NiTi	1h	1.76	78.4	0.91	0.41
	8h	1.96	72.4	0.91	1.17
	24h	1.75	74.2	0.92	2.14
	48h	1.84	76.5	0.92	1.64
	72h	2.22	74.2	0.92	1.15
	96h	2.35	74.0	0.93	0.97
	120h	1.54	73.7	0.92	0.19
Laser-welded NiTi	1h	3.07	68.2	0.90	0.52
	8h	3.05	65.6	0.90	0.99
	24h	2.32	54.0	0.92	1.62
	48h	2.16	56.3	0.91	0.40
	72h	2.13	56.9	0.91	0.31

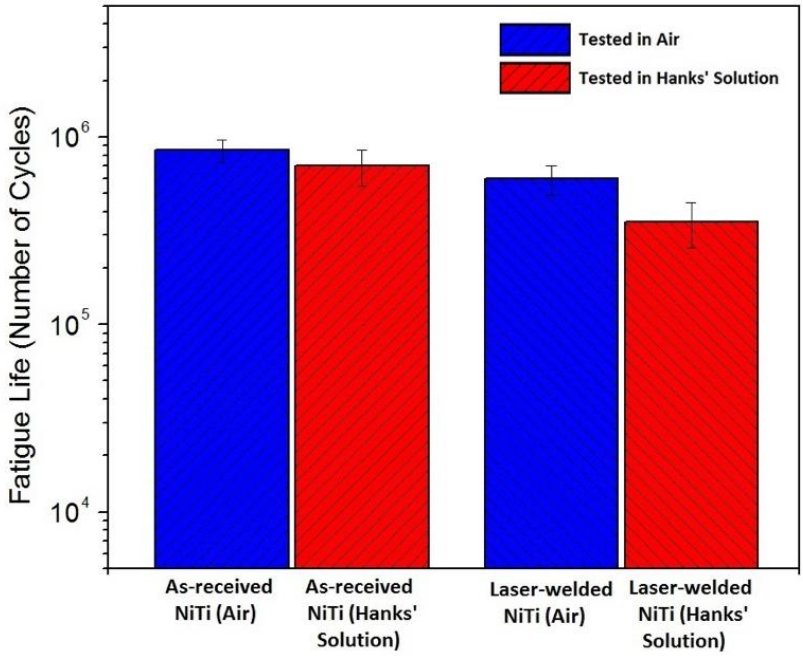

Fig. 1 – Fatigue life measurements for the as-received and laser-welded samples tested by BRF in air and Hanks' solution at 37.5 ^{o}C. The rotational speed and surface strain were kept as 100 rpm (or 1.67 Hz) and 0.42 % respectively.

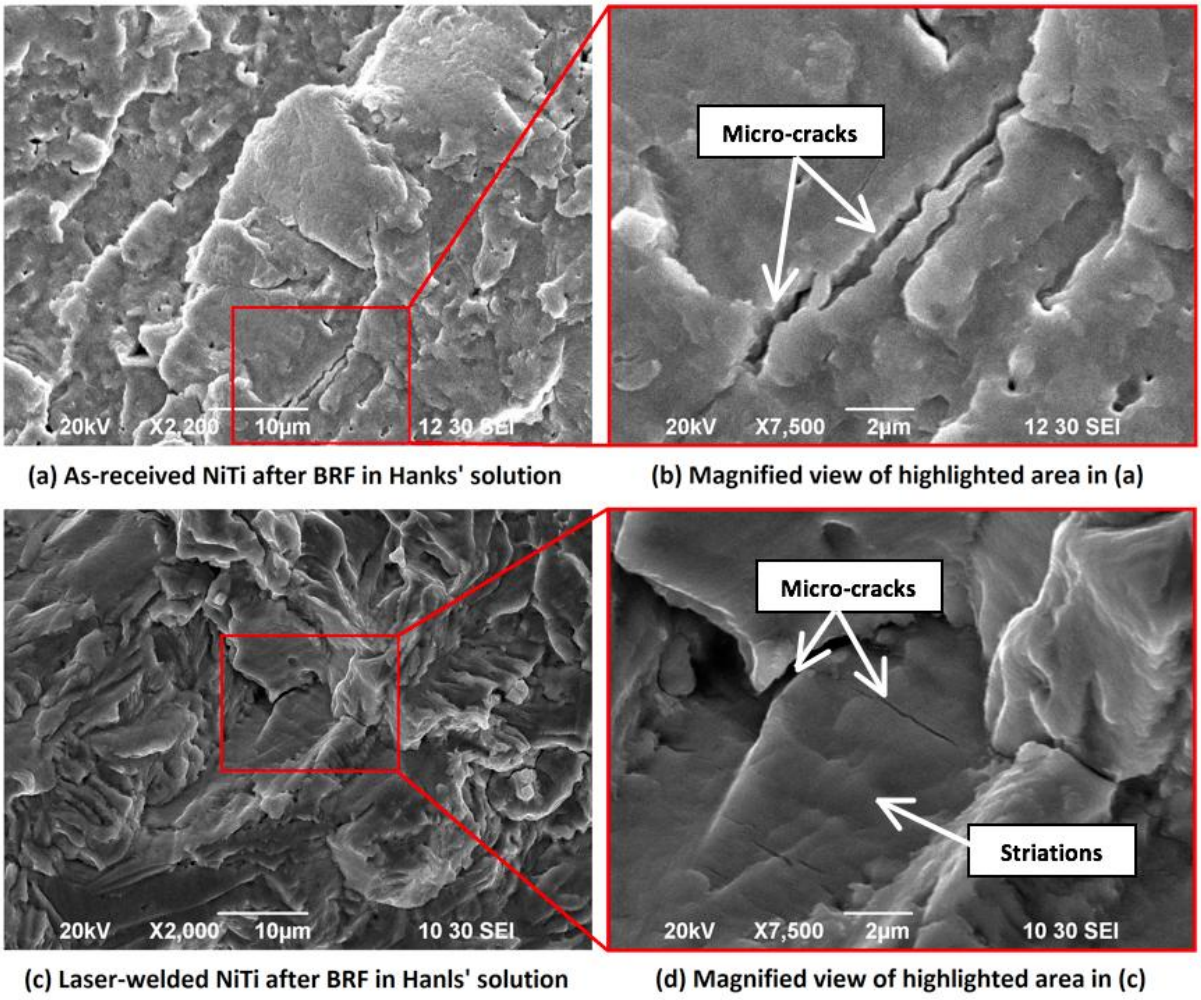

Fig. 2 – SEM fractographs for the (a-b) as-received and (c-d) laser-welded samples after testing by BRF in Hanks' solution at 37.5 ^{o}C.

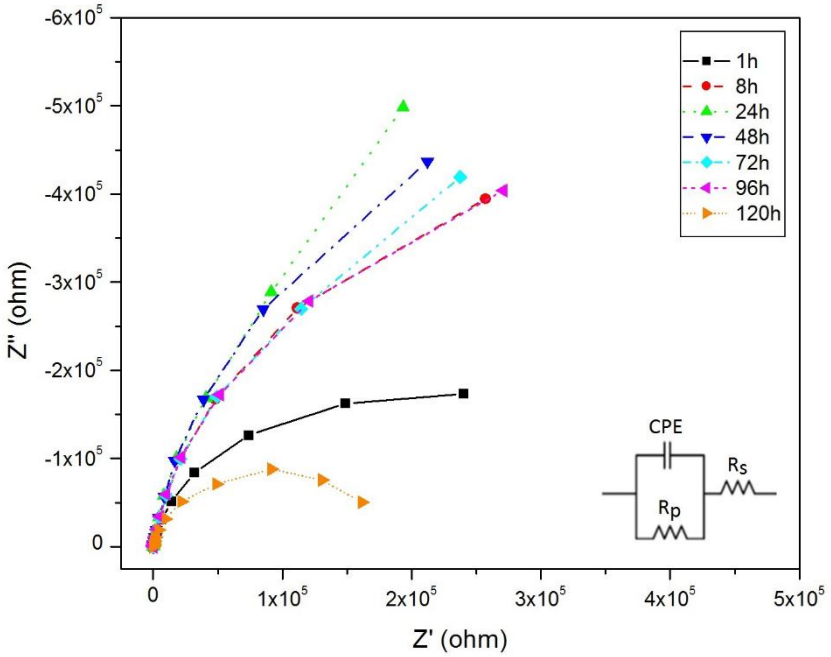

(a) As-received NiTi tested by BRF in Hanks' solution

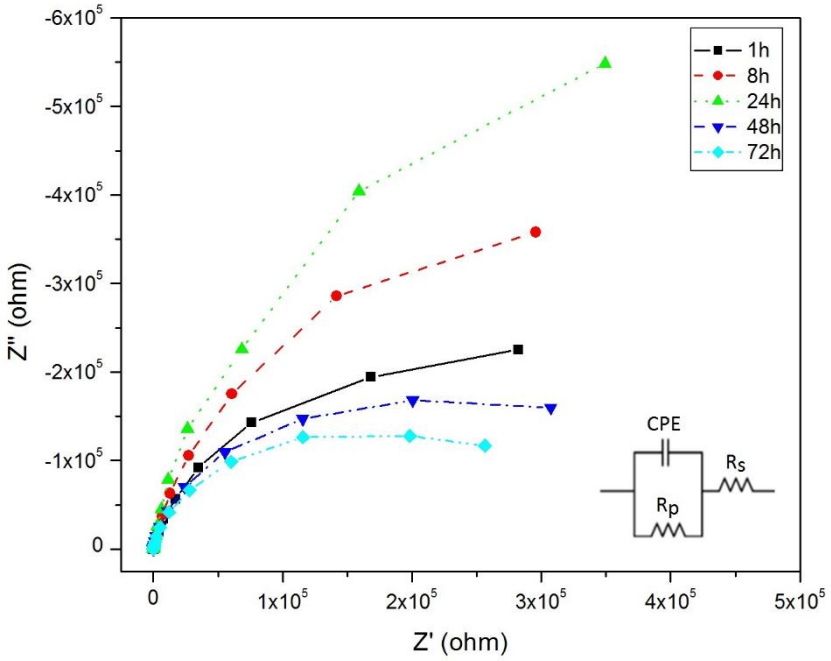

(b) Laser-welded NiTi tested by BRF in Hanks' solution

Fig. 3 – Nyquist plots of the (a) as-received and (b) laser-welded samples after testing by BRF in Hanks' solution at 37.5 ^{o}C with different immersion times. The immersion times vary from 1h to 120h for the as-received sample and 1h to 72h for the laser-welded sample, respectively. The equivalent circuit is provided as an inset in the figure.

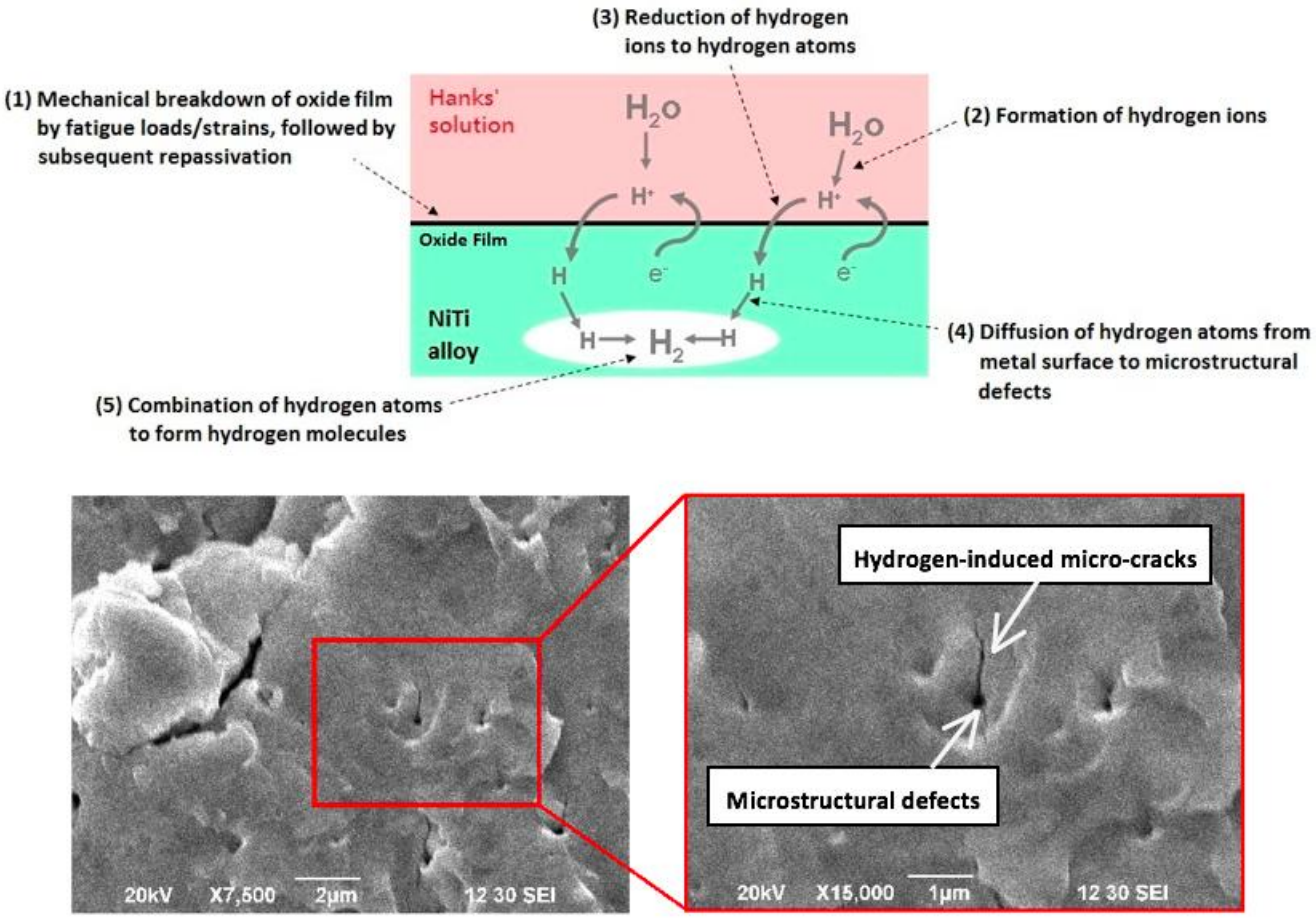

Fig. 4 – Schematic diagram showing the mechanisms for the hydrogen embrittlement in NiTi in Hanks' solution. The SEM fractograph of the as-received NiTi indicates hydrogen-induced cracks originating from the microstructural defects in the metal.

Research Highlights

- Corrosion fatigue was tested by bending rotation fatigue (BRF) in Hanks' solution;
- NiTi laser weldment is susceptible to corrosion fatigue in Hanks' solution;
- Passive film resistance during corrosion fatigue tests were monitored by EIS;
- Reduced fatigue life of NiTi weldment is attributable to hydrogen embrittlement;
- Fatigue fracture occurred in the weld zone (WZ) of the NiTi weldment.